Human Molecular Genetics, 2017, Vol. 26, No. 19 3722–3735

doi: 10.1093/hmg/ddx257
Advance Access Publication Date: 6 July 2017
Original Article

ORIGINAL ARTICLE

Hearing loss without overt metabolic acidosis in ATP6V1B1 deficient MRL mice, a new genetic model for non-syndromic deafness with enlarged vestibular aqueducts

Cong Tian[1,2], Leona H. Gagnon[1], Chantal Longo-Guess[1], Ron Korstanje[1], Susan M. Sheehan[1], Kevin K. Ohlemiller[3], Angela D. Schrader[3], Jaclynn M. Lett[3] and Kenneth R. Johnson[1,*]

[1]The Jackson Laboratory, Bar Harbor, ME 04609, USA, [2]Graduate School of Biomedical Sciences and Engineering, University of Maine, Orono, ME 04469, USA and [3]Department of Otolaryngology, Central Institute for the Deaf, Fay and Carl Simons Center for Hearing and Deafness, Washington University School of Medicine, Saint Louis, MO 63110, USA

*To whom correspondence should be addressed at: The Jackson Laboratory, 600 Main Street, Bar Harbor, ME 04609, USA. Tel: +207 2886228; Fax: +207 2886077; Email: ken.johnson@jax.org

Abstract

Mutations of the human *ATP6V1B1* gene cause distal renal tubular acidosis (dRTA; OMIM #267300) often associated with sensorineural hearing impairment; however, mice with a knockout mutation of *Atp6v1b1* were reported to exhibit a compensated acidosis and normal hearing. We discovered a new spontaneous mutation (vortex, symbol *vtx*) of *Atp6v1b1* in an MRL/MpJ (MRL) colony of mice. In contrast to the reported phenotype of the knockout mouse, which was developed on a primarily C57BL/6 (B6) strain background, MRL-*Atp6v1b1*$^{vtx/vtx}$ mutant mice exhibit profound hearing impairment, which is associated with enlarged endolymphatic compartments of the inner ear. Mutant mice have alkaline urine but do not exhibit overt metabolic acidosis, a renal phenotype similar to that of the *Atpbv1b1* knockout mouse. The abnormal inner ear phenotype of MRL- *Atp6v1b1*$^{vtx/vtx}$ mice was lost when the mutation was transferred onto the C57BL/6J (B6) background, indicating the influence of strain-specific genetic modifiers. To genetically map modifier loci in *Atp6v1b1*$^{vtx/vtx}$ mice, we analysed ABR thresholds of progeny from a backcross segregating MRL and B6 alleles. We found statistically significant linkage with a locus on Chr 13 that accounts for about 20% of the hearing threshold variation in the backcross mice. The important effect that genetic background has on the inner ear phenotype of *Atp6v1b1* mutant mice provides insight into the hearing loss variability associated with dRTA caused by *ATP6V1B1* mutations. Because MRL-*Atp6v1b1*$^{vxt/vtx}$ mice do not recapitulate the metabolic acidosis of dRTA patients, they provide a new genetic model for nonsyndromic deafness with enlarged vestibular aqueduct (EVA; OMIM #600791).

Received: April 6, 2017. **Revised:** June 1, 2017. **Accepted:** June 30, 2017

Introduction

Many of the transport proteins that are involved in acid secretion and bicarbonate reabsorption in the kidney have similar functions in the inner ear (1). The vacuolar (v)H^+-ATPase pump is one of the key membrane transporters for acid excretion in the α-intercalated cells of the distal nephron, and it is also expressed in the inner ear where it functions in endolymph pH homeostasis (2). vH^+-ATPase is a large multi-subunit complex consisting of both cytosolic (V_1) and transmembrane (V_0) domains. Distal renal tubular acidosis (dRTA) caused by vH^+-ATPase mutations (OMIM 267300, 602722) is an autosomal recessive disorder of renal H^+ transport causing a buildup of acid in the bloodstream (metabolic acidosis) with associated alkaline urine; it is frequently accompanied by sensorineural hearing loss. dRTA with hearing loss is caused by mutations in the *ATP6V1B1* gene (2,3), which encodes the B1 subunit of the cytosolic domain of vH^+-ATPase, and with mutations in the *ATP6V0A4* gene (3,4), which encodes the a4 subunit of the transmembrane domain. In contrast to the ubiquitous expression of most other vH^+-ATPase subunits, expression of the B1 and a4 subunits appears to be primarily restricted to the inner ear and kidney, in complexes that mediate H^+ transport across the plasma membrane rather than across the membranes of intracellular organelles (5).

The *Atp6v0a4*$^{-/-}$ knockout mouse, which is on a pure C57BL/6 strain background, recapitulates the systemic metabolic acidosis and hearing loss phenotype seen in human dRTA patients (6,7). In contrast, *Atp6v1b1*$^{-/-}$ knockout mice exhibit a mild compensated acidosis (alkaline urine with impaired handling of an acid load) (8) and have normal hearing (9). A compensatory membrane expression of the vH^+-ATPase B2 subunit was proposed as a possible explanation for why *Atp6v1b1*$^{-/-}$ knockout mice under baseline conditions are healthy and do not exhibit the overt metabolic acidosis and symptoms (growth retardation, failure to thrive) characteristic of dRTA patients with *ATP6V1B1* mutations (8). In support of this hypothesis, B2-containing H^+-ATPase complexes, which normally localize to intracellular organelles, were shown to relocalize to the apical membranes of renal intercalated cells in B1-deficient *Atp6v1b1*$^{-/-}$ knockout mice (10).

In the mouse inner ear, *Atp6v1b1* expression has been detected in the epithelial cells of the endolymphatic sac and duct and in the interdental cell layer of the cochlear spiral limbus (2,9). The inner ear expression pattern and the deafness that is associated with *ATP6V1B1* mutations in human dRTA patients suggest that ATP6V1B1 plays an important role in pH balance in the mouse inner ear. The surprising finding that *Atp6v1b1*$^{-/-}$ knockout mice have normal hearing (9), however, implies that redundant mechanisms of pH regulation can compensate for the loss of the vH^+-ATPase B1 subunit in the mouse inner ear. This compensation may come from relocalization of B2-containing vH^+-ATPase complexes from intracellular to apical membranes as proposed for renal cells, or it may be accomplished by other acid-base transporting mechanisms or pH buffering systems in the inner ear.

Here, we describe the genetic and phenotypic characterization of a new spontaneous mouse mutation of the *Atp6v1b1* gene, named vortex (*vtx*) for the circling behavior that first identified mutant mice. Mice homozygous for this recessive mutation exhibit auditory and vestibular dysfunction associated with enlarged endolymphatic compartments of their inner ears, phenotypic features that were not observed in the previously reported *Atp6v1b1*$^{-/-}$ knockout mouse (9) but that are similar to those of *Atp6v0a4*$^{-/-}$ knockout mice (6). Mice homozygous for a genetically engineered *Atp6v1b1*^{tm1}knockout allele, produced by replacing exons 7–11 with a Neo cassette, were characterized on a primarily C57BL/6 (B6) background with some admixture from 129S1-derived CJ7 ES cells (8), whereas the spontaneous *Atp6v1b1*^{vtx} missense mutation arose on the genetically distinct MRL/MpJ (MRL) strain. We show by congenic strain analysis that the differences in inner ear phenotypes between MRL-*Atp6v1b1*$^{vtx/vtx}$ and B6(129S1)-*Atp6v1b1*$^{-/-}$ knockout mice are due to strain background differences and not to differences in the natures of their *Atp6v1b1* mutations. We exploited these strain-specific differences in a linkage backcross to map loci that modify the degree of hearing loss in *Atp6v1b1*$^{vtx/vtx}$ mice and found statistically significant linkage with Chromosome 13 markers. The results of our studies in mice provide insight into the hearing loss variability that is associated with human *ATP6V1B1* mutations and suggest that genetic background effects underlie this variation. Because MRL-*Atp6v1b1*$^{vtx/vtx}$ mice exhibit enlargements of the endolymphatic sac and duct in the inner ear but do not exhibit the overt metabolic acidosis characteristic of dRTA, they provide a new genetic model for nonsyndromic deafness with enlarged vestibular aqueducts (EVA; OMIM 600791).

Results

Genetic mapping of the *vtx* mutation

The vortex (*vtx*) mutation arose spontaneously in a colony of MRL/MpJ (MRL) mice at The Jackson Laboratory. Mice homozygous for *vtx* are healthy and fertile with normal growth, but they exhibit vestibular dysfunction as evidenced by variable head tilting and circling behaviors, and they are profoundly hearing impaired as shown by ABR analysis (Fig. 1A).

We first attempted to genetically map *vtx* by generating an intercross of MRL-*vtx* mice with B6 mice; however, the cross was terminated because no abnormal vestibular-related behaviors were observed in multiple litters of F2 progeny from this cross. A second linkage intercross then was made with F1 hybrids between MRL-*vtx/vtx* mice and FVB/NJ (FVB) strain mice. Although the number of mutant (*vtx/vtx*) F2 progeny from this intercross, identified by elevated ABR thresholds, was less than expected, 18 were eventually produced (out of a total of 164 F2s) and used for a genome-wide linkage screen with MIT microsatellite markers that differed in size between MRL and FVB. Results of this low-resolution screen indicated linkage of the *vtx* phenotype with markers *D6Mit15* (17% recombination) and *D6Mit366* (11% recombination) on Chr 6.

To verify and refine this linkage association, a backcross of (MRL-*vtx/vtx* x FVB) F1 hybrids to MRL-*vtx/vtx* mice was used to generate a total of 101 N2 progeny. Presumed genotypes (+/*vtx* or *vtx/vtx*) of the N2 mice were assigned according to their ABR thresholds. The distribution of ABR thresholds among N2 mice was strongly bimodal (Fig. 1B) as expected for a primarily monogenic trait. About half (59) of the 101 N2 backcross mice had 16 kHz thresholds equal to or less than 30 dB SPL (assigned +/*vtx* genotypes) and about half (42) had thresholds equal to or greater than 40 dB SPL (assigned *vtx/vtx* genotypes). Thresholds for 8 and 32 kHz stimuli were also analysed to reinforce genotype assignments. The wide range of ABR thresholds among N2 mice in the *vtx/vtx* category (Fig. 1B) suggests the influence of strain-specific modifiers, which may explain why so few mutant phenotypes were observed in progeny from the (MRL x FVB)-+/*vtx* intercross. The N2 mice then were genotyped for multiple

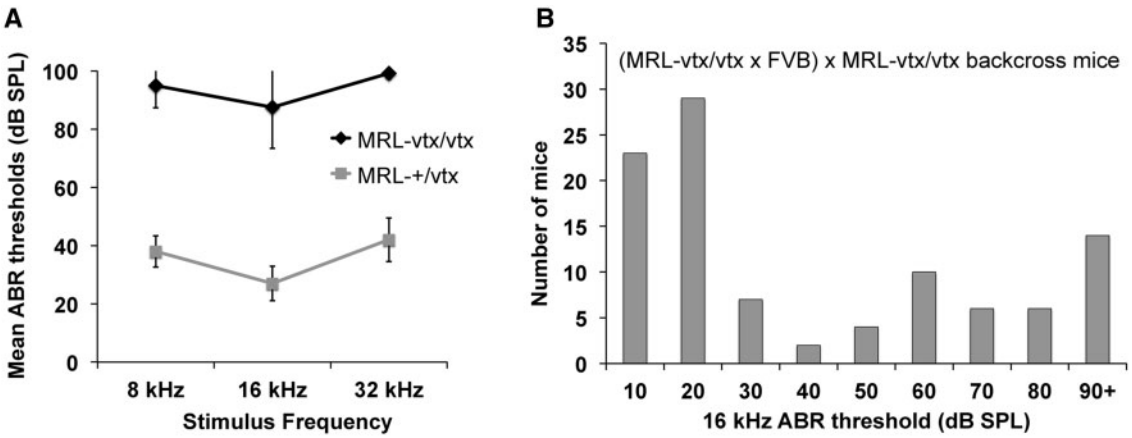

Figure 1. ABR thresholds of MRL-*vtx/vtx* mutant mice and linkage backcross mice. (**A**) Average ABR thresholds of six (4 females, 2 males) MRL-*vtx/vtx* mutant mice and ten MRL-+/*vtx* control mice for 8, 16, and 32 kHz pure tone stimulus frequencies. All mice were tested between 4 and 6 weeks of age. Error bars represent standard deviations. Thresholds were assigned a value of 100 if no ABR was obtained at the maximum test stimulus of 100 dB SPL. (**B**) Frequency distribution of 16 kHz ABR thresholds among 101 N2 mice of the (MRL-*vtx/vtx* x FVB) x MRL-*vtx/vtx* backcross. About half of the N2 mice are expected to be genotype +/*vtx* and half *vtx/vtx*.

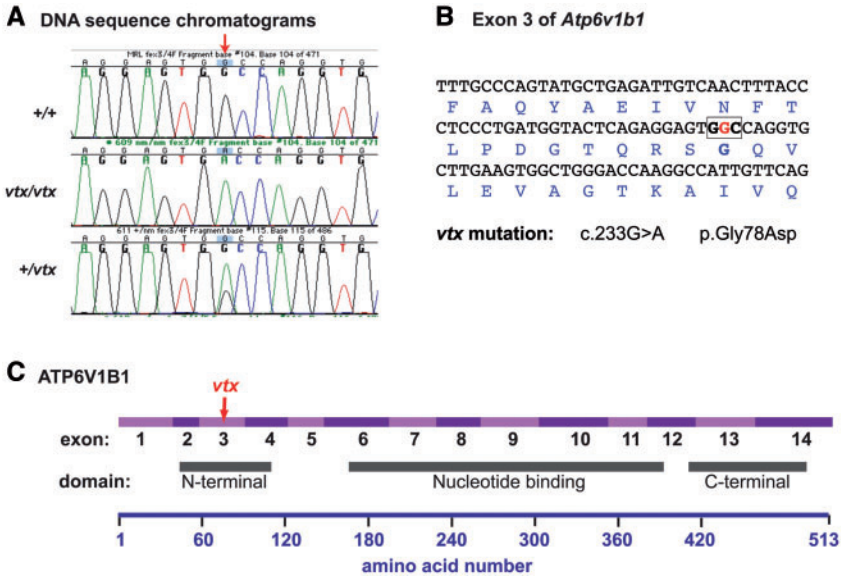

Figure 2. Molecular characterization and consequences of the *Atp6v1b1*^{vtx} mutation. (**A**) DNA sequence chromatograms illustrating the G > A nucleotide change (indicated by red arrow) caused by the *vtx* mutation. (**B**) DNA sequence of *Atp6v1b1* exon 3 with encoded amino acids shown below in blue font. The G nucleotide that is altered in the *vtx* mutation (shown in red) is part of the GGC codon (boldface, boxed) for glycine. The G > A nucleotide substitution at coding DNA position 233 (c.233G > A) causes a glycine to aspartic acid amino acid change at position 78 of the ATP6V1B1 protein (p.Gly78Asp). (**C**) Schematic diagram of the ATP6V1B1 protein showing the regions encoded by exons 1–14 in alternating light and dark purple shades and locations of the three functional domains relative to the amino acid numbers shown below. The *vtx* mutation is in exon 3, which encodes part of the N-terminal domain of the protein.

polymorphic SNP markers on Chr 6, and haplotype analysis refined the *vtx* candidate region to the interval between *rs13478778* (Chr6: 58,317,346 bp; GRCm38) and *rs3708822* (Chr6: 89,292,518 bp).

Gene identification and molecular characterization of the *vtx* mutation

The 31 Mb candidate region for the *vtx* mutation contains the *Atp6v1b1* gene (Chr6: 83,742,990 bp-83,758,855 bp), which encodes the B1 subunit of the vacuolar H^+-ATPase. We considered *Atp6v1b1* a good candidate gene for the *vtx* mutation because (1) it is expressed in the inner ear (2), mutations of the human *ATP6V1B1* and *ATP6V0A4* genes cause dRTA and deafness, and (3) the inner ear phenotype of *vtx/vtx* mutant mice is similar to that of *Atp6v0a4* knockout mice (6,7). The genomic DNA sequences of all 14 *Atp6v1b1* exons and their flanking splice sites in MRL-*vtx/vtx* mutant mice were compared with those of MRL wildtype controls and revealed a single base pair mutation in exon 3 (c.233G > A) that changes the codon for glycine (GGC) to a codon for aspartic acid (GAC) at amino acid position 78 (p.G78D) of the mouse protein (Fig. 2). DNA sequence analysis of exon 3 in additional mutant ($N = 15$) and non-mutant ($N = 7$) mice confirmed this variant to be the recessive *Atp6v1b1*^{vtx} mutation. The *vtx* missense mutation occurs in the N-terminal domain of ATP6V1B1 (InterPro: IPR004100).

The early onset, profound hearing impairment of *Atp6v1b1*$^{vtx/vtx}$ mice on the MRL strain background (Fig.1A) is

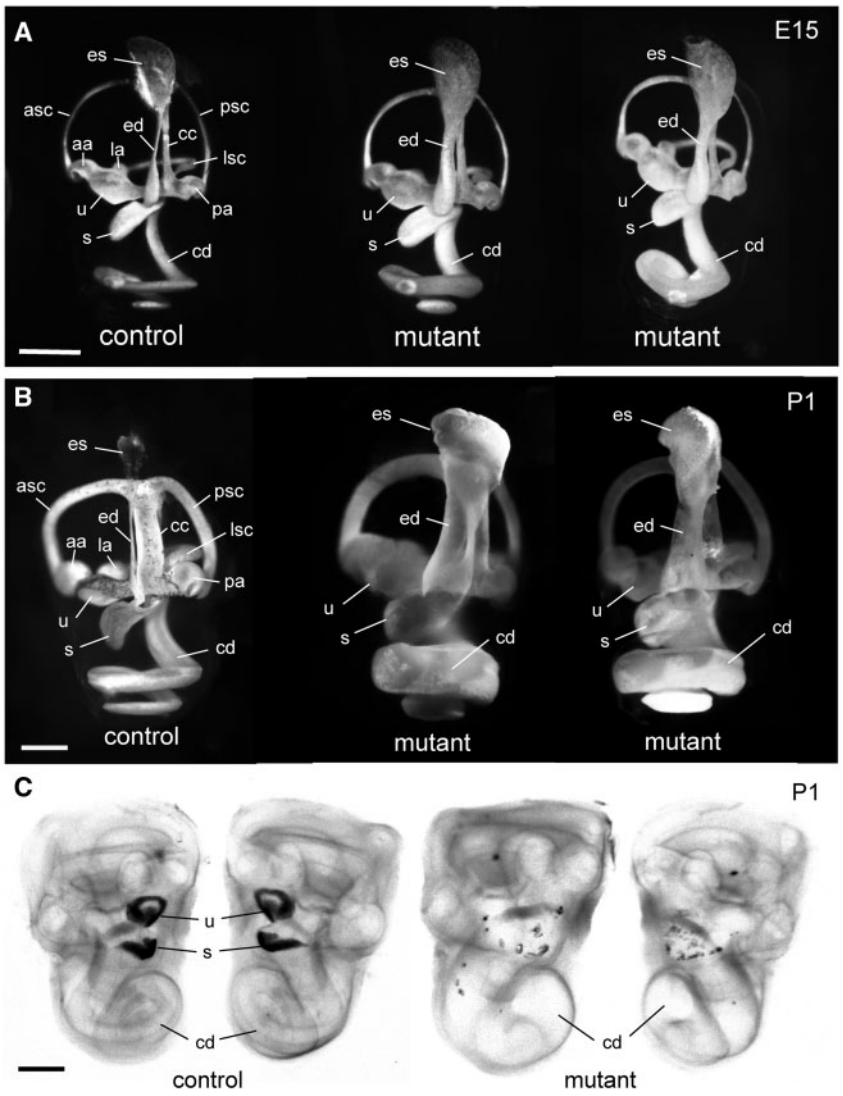

Figure 3. Paint fills and whole mounts of inner ears from MRL-*Atp6v1b1*$^{vtx/vtx}$ mutant and control mice. (**A**) Paint fills of the membranous labyrinths of inner ears from an E15-stage MRL-*Atp6v1b1*$^{+/vtx}$ (control) embryo and two littermate MRL-*Atp6v1b1*$^{vtx/vtx}$ (mutant) embryos. The endolymphatic sac (es), endolymphatic duct (ed), utricle (u), saccule (s), and cochlear duct (cd) appear enlarged in the two mutant inner ears compared with the control. (**B**) Paint fills of the membranous labyrinths of inner ears from a newborn (P1) MRL-*Atp6v1b1*$^{+/vtx}$ (control) mouse and two MRL-*Atp6v1b1*$^{vtx/vtx}$ (mutant) littermates. The entire membranous labyrinth of the mutant inner ears appears swollen from an excess of endolymph. Other structures labeled in the control inner ears of A and B: anterior semicircular canal (asc), posterior semicircular canal (psc), lateral semicircular canal (lsc), anterior ampulla (aa), posterior ampulla (pa), lateral ampulla (la), common crus (cc). (**C**) Cleared, whole-mount preparations of both inner ears from a P1 *Atp6v1b1*$^{+/vtx}$ newborn mouse (control) and two MRL-*Atp6v1b1*$^{vtx/vtx}$ (mutant) littermates, illuminated from below. Dark-appearing otoconia in the utricle (u) and saccule (s) are clearly visible in the control ear, but only a few widely dispersed otoconial crystals are seen in the mutant inner ears. The cochlear ducts (cd) of the mutant inner ears are enlarged compared with the control. Scale bars for A, B, C: 0.5 mm.

strikingly different from the previously reported normal auditory phenotype of *Atp6v1b1*$^{-/-}$ knockout mice on a mixed B6/129S1 strain background (9). To specifically test for MRL versus B6 strain background effects on the mutant phenotype, we generated B6.MRL-*Atp6v1b1*$^{vtx/vtx}$ congenic mice (described in Materials and Methods) and compared their inner ear and kidney phenotypes with those of MRL-*Atp6v1b1*$^{vtx/vtx}$ mice.

Inner ear morphology and auditory function

Paintfills of the membranous labyrinths of inner ears from MRL-*Atp6v1b1*$^{vtx/vtx}$ mutants and controls were examined in day 15 embryos (E15) and in newborn (P1) mice. Already at E15, the membranous labyrinth of MRL-*Atp6v1b1*$^{vtx/vtx}$ embryos appeared dilated compared with inner ears of MRL-*Atp6v1b1*$^{+/vtx}$ littermate controls. The swelling was especially apparent in the endolymphatic sac and duct, but also noticeable in the utricle, saccule, and cochlear duct (Fig. 3A). The enlargement of the membranous labyrinth in inner ears of MRL-*Atp6v1b1*$^{vtx/vtx}$ mutant mice became even more pronounced at P1 (Fig. 3B). Cleared whole-mount preparations of inner ears from newborn MRL-*Atp6v1b1*$^{vtx/vtx}$ mice showed an obvious enlargement of the cochlear duct but also showed a conspicuous deficiency and dispersion of utricular and saccular otoconia compared with MRL-*Atp6v1b1*$^{+/vtx}$ littermate control mice (Fig. 3C). Whole mount preparations of inner ears from B6.MRL- *Atp6v1b1*$^{vtx/vtx}$ mice showed normal morphology, indistinguishable from that of the parental B6 strain mice.

Cross-sections of plastic-embedded adult (2.5–4.5 months-of-age) cochleae (Fig. 4) revealed differences in the arrangement

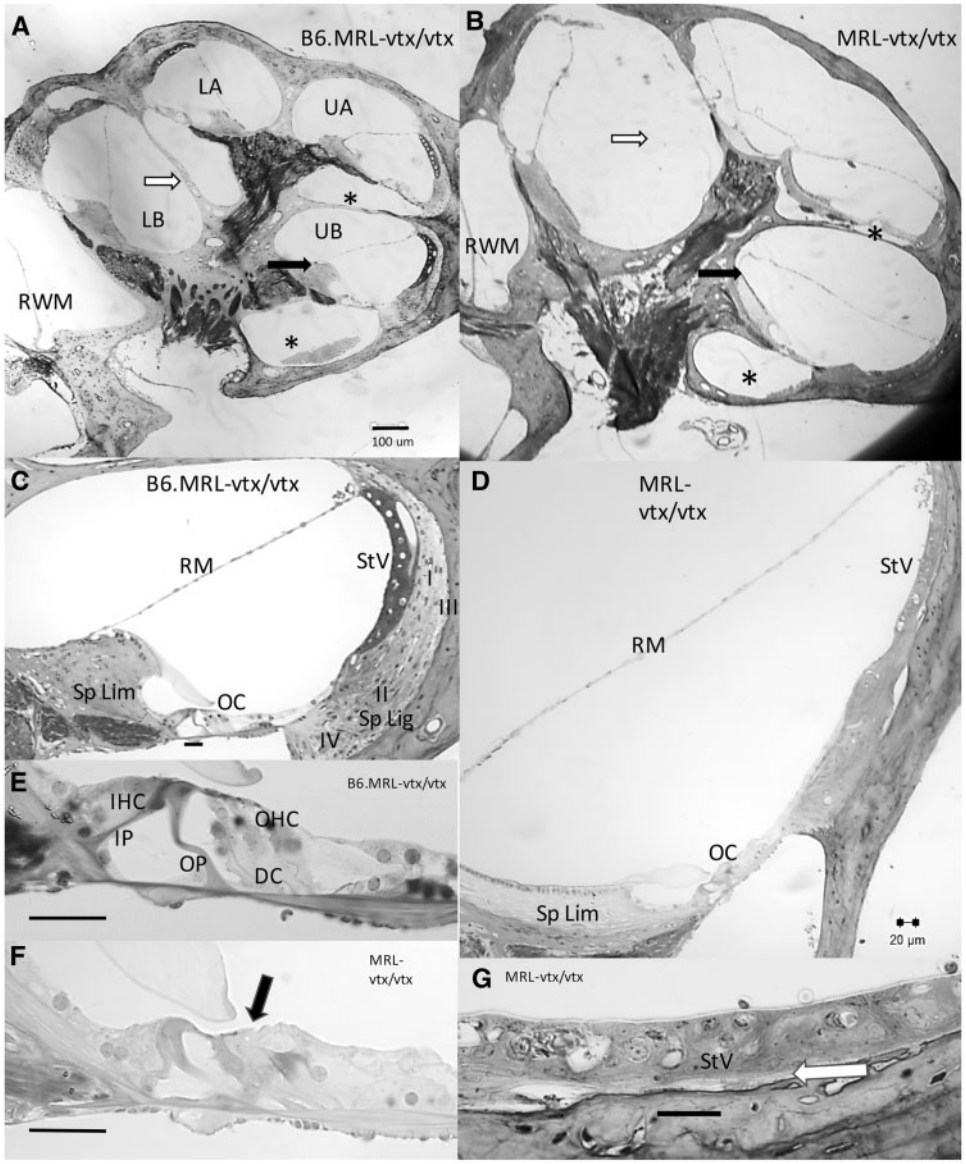

Figure 4. Cross sections of cochleae from B6.MRL-*Atp6v1b1*$^{vtx/vtx}$ and MRL-*Atp6v1b1*$^{vtx/vtx}$ mice. (**A, B**) Whole cochlear profiles from B6.MRL-*Atp6v1b1*$^{vtx/vtx}$ (A) and MRL-*Atp6v1b1*$^{vtx/vtx}$ mice (B) imaged at the same magnification. B6.MRL-*Atp6v1b1*$^{vtx/vtx}$ mutants appear normal while MRL-*Atp6v1b1*$^{vtx/vtx}$ mutants feature greatly reduced scala tympani (compare areas marked with *), missing interscalar septum between lower base and lower apex (compare areas marked with white arrows), and differences in the shape of spiral limbus and attachment point of Reissner's membrane (compare black arrows). (**C, D**) Upper basal turn scala media profiles from different specimens of B6.MRL-*Atp6v1b1*$^{vtx/vtx}$ (C) and MRL-*Atp6v1b1*$^{vtx/vtx}$ mice (D) imaged at the same magnification. B6.MRL-*Atp6v1b1*$^{vtx/vtx}$ mutants appear normal while MRL-*Atp6v1b1*$^{vtx/vtx}$ mutants show widened profile, elongated and acellular spiral limbus, hair cell loss (see **E, F**), and spiral ligament degeneration (see **G**). (E, F) Enlarged views of organ of Corti from C,D show outer hair cell loss in MRL-*Atp6v1b1*$^{vtx/vtx}$ mutant (black arrows). (G) Enlarged view of MRL-*Atp6v1b1*$^{vtx/vtx}$ mutant stria vascularis from D shows thin and somewhat disorganized stria with near absence of type I and III fibrocytes (white arrow). Scale bar in A applies to B. All other scale bars 20 μm. LB, Lower base; UB, Upper base; LA, Lower apex; UA, Upper apex; RWM, Round window membrane; Sp Lim, Spiral Limbus; Sp Lig, Spiral ligament; RM, Reissner's membrane; StV, Stria vascularis; I, II, III, IV, Fibrocyte types by area; OC, Organ of Corti; IP, Inner pillar; OP, Outer pillar; DC, Deiters' cells; IHC, Inner hair cell; OHC, Outer hair cell.

of cochlear fluid spaces in B6.MRL-*Atp6v1b1*$^{vtx/vtx}$ and MRL-*Atp6v1b1*$^{vtx/vtx}$ mutant mice. This could be characterized as a lateral expansion of fluid spaces (transverse to the modiolus), basal displacement of the organ of Corti, and reduction in size of scala tympani in the mutants. Scala media appeared expanded, partly by virtue of displacement of the attachment point of Reissner's membrane to the medial side of a greatly elongated spiral limbus. The spiral limbus also had a stubby, misshapen profile and often contained few fibrocytes, especially apically. At the ages examined, apical bulging of Reissner's membrane was subtle, except for two mice (not shown) where Reissner's membrane pressed up against the walls of the boney labyrinth, nearly eliminating scala vestibuli. Spiral ligament was extremely thin throughout the cochlea. Type I and III fibrocytes were almost entirely missing behind the stria. The stria was also typically thin, especially basally, yet overall, strial structure appeared largely preserved. Most noteworthy was the frequent absence of the boney interscalar septum between the lower cochlear base and lower apical turn. The septum appeared fused with the osseous spiral lamina of the adjacent cochlear regions. Inner hair cells were mostly preserved in the mutants, as were afferent neurons, except in the two extreme

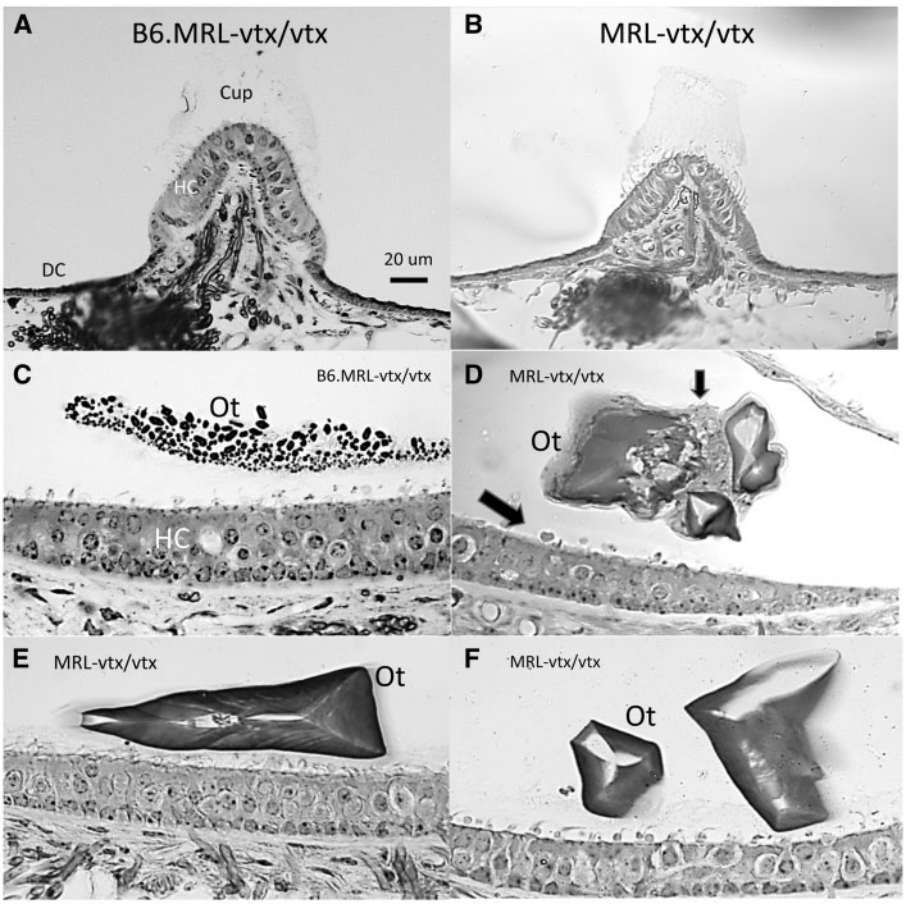

Figure 5. Cross sections of vestibular organs from B6.MRL-*Atp6v1b1*$^{vtx/vtx}$ and MRL-*Atp6v1b1*$^{vtx/vtx}$ mice. **(A, B)** Both B6.MRL-*Atp6v1b1*$^{vtx/vtx}$ (A) and MRL-*Atp6v1b1*$^{vtx/vtx}$ (B) mutant cristae appear normal (posterior cristae is shown), including presence of cupula, hair cells, and dark cells. **(C–F)** B6.MRL-*Atp6v1b1*$^{vtx/vtx}$ maculae (saccule shown in C) appear normal. MRL-*Atp6v1b1*$^{vtx/vtx}$ mutant maculae (saccule is shown in D-F) show normal complement of hair cells, but few, very large otoconia that tend toward triangular shapes. Possible macrophages (arrows in D) line the epithelial surface and surround abnormal otoconia. Scale bar in A applies to all panels. Cup, Cupula; HC, Hair cells; DC, Dark cells; Ot, Otoconia.

hydropic mice, which showed pronounced atrophy of the organ of Corti. In the other mutants, outer hair cells were generally absent in the cochlear base, but present to a variable extent in the apex.

Comparison of the vestibular organs by genotype (Fig. 5) indicated little hair cell or neural loss in any group. MRL-*Atp6v1b1*$^{vtx/vtx}$ mutant cristae were similar to those of the B6.MRL-*Atp6v1b1*$^{vtx/vtx}$ mutants in normal appearance, including the presence of a cupula and complement of dark cells. The appearance of most maculae was likewise similar across genotypes with respect to hair cells. Exceptions were atrophic saccular maculae of the two most hydropic mice. The most striking vestibular abnormality of the MRL-*Atp6v1b1*$^{vtx/vtx}$ mutants was the presence, principally in the saccule, of few but very large otoconia that tended toward triangular shapes. These were often associated with possible macrophages. Perhaps due to faulty attachment, the large otoconia were observed in cochlear scala media in 5 of 9 mutants. No otoconia were observed covering the utricular maculae, although it cannot be ruled out that these were more prone to migrate during processing.

ABR thresholds of adult mice (2.5 and 4.5 months of age) were compared for 5, 10, 20, 28.3, 40, and 56.6 kHz test stimuli (Fig. 6A). Thresholds of B6.MRL-*Atp6v1b1*$^{vtx/vtx}$ congenic strain mice and MRL-*Atp6v1b1*$^{+/vtx}$ control mice were similar and in the normal range for most inbred mouse strains. MRL-*Atp6v1b1*$^{vtx/vtx}$ mice, however, failed to elicit an ABR even at the maximum test stimulus (100 dB SPL) for any of the test frequencies, indicating complete deafness. Likewise, EP measurements were normal in B6.MRL-*Atp6v1b1*$^{vtx/vtx}$ and MRL-*Atp6v1b1*$^{+/vtx}$ mice but nearly absent in MRL-*Atp6v1b1*$^{vtx/vtx}$ mice (Fig. 6B). These results clearly demonstrate that the MRL strain background has a strong deleterious effect on the auditory phenotype of *Atp6v1b1*$^{vtx/vtx}$ mutant mice.

Kidney-related phenotype

MRL-*Atp6v1b1*$^{vtx/vtx}$ and B6.MRL-*Atp6v1b1*$^{vtx/vtx}$ mice were healthy and showed no overt symptoms of metabolic acidosis. The previously reported B6(129S1)-*Atp6v1b1* knockout mice show increased urine pH, decreased calcium excretion, and decreased urine osmolality (9). We measured these characteristics in the MRL-*Atp6v1b1*$^{vtx/vtx}$ and B6.MRL-*Atp6v1b1*$^{vtx/vtx}$ mice and compared them with wildtype mice from the same genetic background. Similar to results reported for mice with the *Atp6v1b1* knockout mutation, mice homozygous for the *Atp6v1b1*^{vtx} mutation on the B6 background had a significantly higher urine pH (6.5 ± 0.1 vs 6.2 ± 0.1) compared to wildtype B6 mice (Fig. 7A). We did not observe a difference between wildtype and *Atp6v1b1*$^{vtx/vtx}$ mutant mice on the MRL background, but wildtype MRL mice had an unusually high urine pH (6.5 ± 0.2)

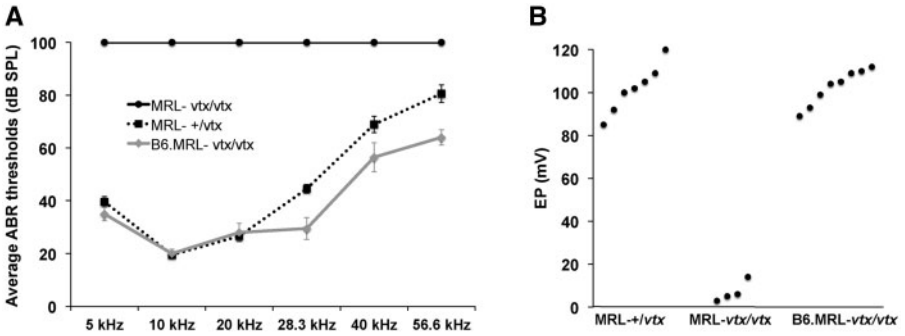

Figure 6. ABR and EP measurements of auditory function in B6.MRL-*Atp6v1b1*$^{vtx/vtx}$ and MRL-*Atp6v1b1*$^{vtx/vtx}$ mice. (**A**) Average ABR thresholds of MRL-*Atp6v1b1*$^{vtx/vtx}$ mice (MRL-vtx/vtx; 4 females, 6 males); MRL-*Atp6v1b1*$^{+/vtx}$ mice (MRL-$^{+/vtx}$; 3 females, 5 males); and B6.MRL-*Atp6v1b1*$^{vtx/vtx}$ mice (B6.MRL-vtx/vtx; 5 females, 5 males). Thresholds were obtained from 5, 10, 20, 28.3, 40, and 56.6 kHz pure tone test frequencies. Thresholds were assigned a value of 100 if no ABR was obtained at the maximum test stimulus of 100 dB SPL. Mice were tested between 2.5 and 4.5 months of age. Bars represent standard errors of the means. (**B**) Enodocochlear potential (EP) measurements (mV) of the same mice were obtained immediately after the ABR tests. EP values are shown for individual mice. Only the four EP measurements in MRL-*Atp6v1b1*$^{vtx/vtx}$ mice that were verified to have correct electrode placements are shown.

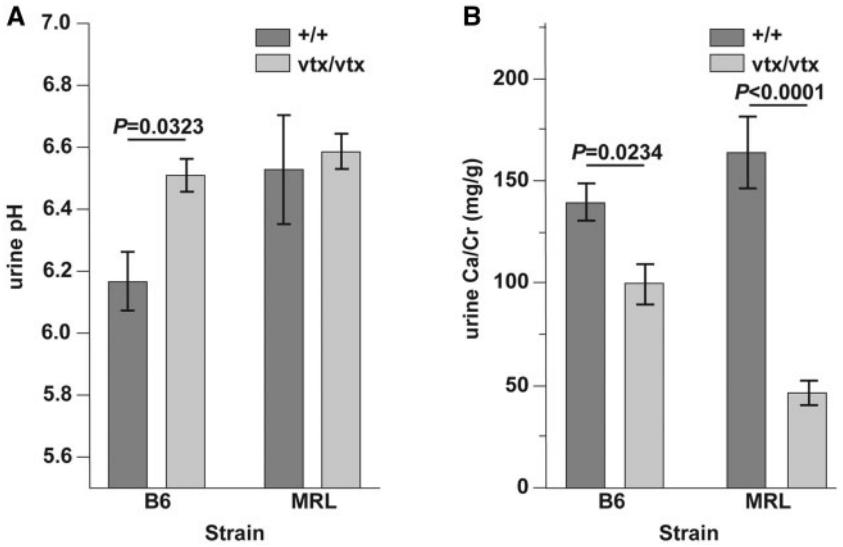

Figure 7. Renal secretion in B6- and MRL-*Atp6v1b1*^{vtx} mutant mice at 17 weeks of age. (**A**) Urine alkalinity is significantly increased in *vtx* mice compared to wildtype controls in the B6 background, but not in the MRL background. Urine pH of MRL$^{+/+}$ mice is significantly higher than that of B6$^{+/+}$ mice and similar to that of *vtx/vtx* mutant mice on either strain background. (**B**) Calcium excretion is decreased in the mutant mice for both genetic backgrounds, but with a much larger decrease in MRL. Values are expressed as mean ± SE and each group contained 5 male mice. The Student's paired t-test with two-tailed distribution was used to determine the statistical probabilities shown in A and B.

compared to several other strains we tested: C57BL/6J (6.2 ± 0.1), A/J (6.1 ± 0.1), 129S1/SvImJ (5.8 ± 0.1), and NOD/LtJ (6.0 ± 0.2).

Decreased calcium excretion (urinary Ca^{2+}/Cr mg/g ratios) was observed in mice with the *Atp6v1b1*^{vtx} mutation in both genetic backgrounds (Fig. 7B) although we saw a larger decrease (163.3 ± 17.4 vs. 45.9 ± 6.0l, approx. 70%) in the MRL background compared to the B6 background (139.2 ± 9.1 vs. 99.0 ± 9.6, approx. 30%). We did not measure a significant effect of the *Atp6v1b1*^{vtx} mutation on urine osmolality on either background. In addition, we also measured potassium, sodium, and chloride concentrations in both blood and urine and did not find any significant differences between *Atp6v1b1*$^{vtx/vtx}$ and wildtype mice on either strain background (Table 1).

Genetic mapping of hearing loss modifiers

To genetically map loci that contribute to hearing loss differences between B6.MRL-*Atp6v1b1*$^{vtx/vtx}$ and MRL-*Atp6v1b1*$^{vtx/vtx}$

Table 1. Physiological parameters of *Atp6v1b1*$^{vtx/vtx}$ (*vtx/vtx*) and *Atp6v1b1*$^{+/+}$ (+/+) control mice on the MRL and B6 strain backgrounds. There were no statistically significant differences between mutant and wildtype mice from the same genetic background

	MRL		B6	
	+/+	*vtx/vtx*	+/+	*vtx/vtx*
Blood				
Na^+, mM	156.4 ± 0.7	155.3 ± 1.0	151.5 ± 1.5	154.1 ± 0.9
K^+, mM	5.6 ± 0.1	6.6 ± 0.7	5.2 ± 0.2	5.9 ± 0.4
Cl^-, mM	104.4 ± 0.6	106.4 ± 1.2	110.1 ± 0.8	109.7 ± 0.7
Osm, mmol/kg	326 ± 3	323 ± 3	328 ± 2	320 ± 2
Urine				
Na^+, mM	173.2 ± 42.1	142.8 ± 22.6	152.0 ± 15.8	154.6 ± 27.5
K^+, mM	155.9 ± 27.7	136.4 ± 9.0	166.6 ± 16.5	157.4 ± 5.4
Cl^-, mM	155.3 ± 34.6	134.5 ± 14.2	177.4 ± 19.6	167.4 ± 21.7
Osm, mmol/kg	993 ± 106	896 ± 139	1,026 ± 185	1,069 ± 254

Values are mean ± SE. The number of male mice in each group is 5.

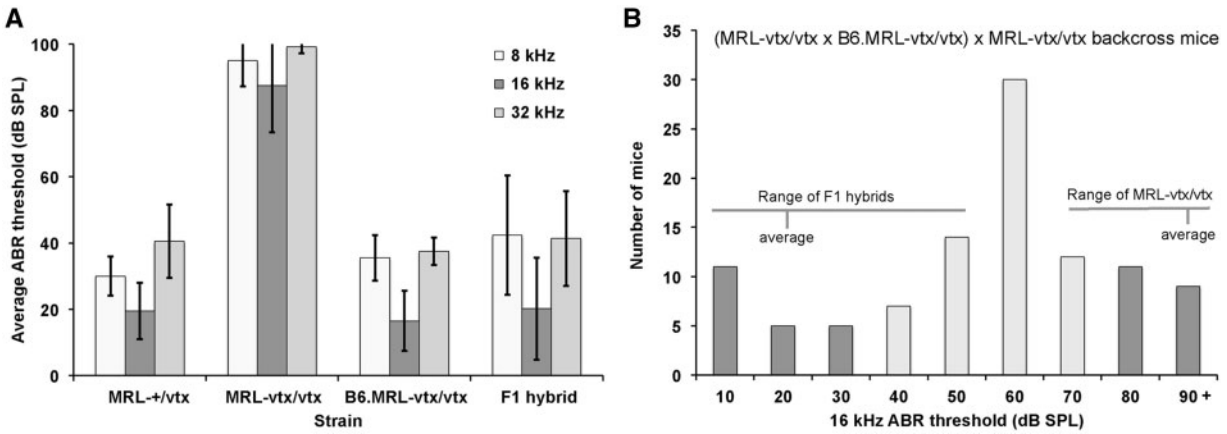

Figure 8. ABR thresholds of parental strains, F1 hybrids, and N2 backcross mice. (**A**) Average ABR thresholds of MRL-*Atp6v1b1*$^{+/vtx}$ controls (MRL-+/vtx, $N = 11$, test age 5 wks); MRL-*Atp6v1b1*$^{vtx/vtx}$ mutant mice (MRL-vtx/vtx; $N = 6$, test age 5 wks); B6.MRL-*Atp6v1b1*$^{vtx/vtx}$ congenic mice (B6.MRL-vtx/vtx; $N = 10$, test age 8 wks); and MRL-*Atp6v1b1*$^{vtx/vtx}$ x B6.MRL-*Atp6v1b1*$^{vtx/vtx}$ F1 hybrid mice ($N = 31$, test age 6 wks). Thresholds were assigned a value of 100 if no ABR was obtained at the maximum test stimulus of 100 db SPL. Error bars represent standard deviations of the means to illustrate the extent of the within group variation. The post-hoc Tukey test, which controls for multiple pair-wise comparisons, was used to determine the statistical significance of mean differences between pairs of strains. For all test frequencies, the mean ABR thresholds of the MRL-*vtx/vtx* strain were statistically significantly higher ($P < 0.001$) than the means of the other three strains, which were not significantly different from each other ($P > 0.5$). (**B**) Distribution of 16 kHz ABR thresholds among 102 backcross (N2) mice generated from matings of (MRL-*Atp6v1b1*$^{vtx/vtx}$ x B6.MRL-*Atp6v1b1*$^{vtx/vtx}$) F1 hybrids with MRL-*Atp6v1b1*$^{vtx/vtx}$ mice. All N2 mice (genotype *Atp6v1b1*$^{vtx/vtx}$) were tested for ABR thresholds at 4-6 weeks of age. The dark colored bars on the ends of the distribution indicate 40 N2 mice with the most extreme thresholds, which were used for whole-genome linkage analysis to map modifier loci.

mutant mice, we first generated F1 hybrids between these two strains. The F1 hybrid mice are homozygous for the *vtx* mutation and for MRL alleles at linked loci within the congenic region of the B6.MRL-*Atp6v1b1*$^{vtx/vtx}$ strain, and heterozygous for B6 and MRL alleles elsewhere in the genome. ABR thresholds of 6-week-old F1 hybrids are very similar to those of 8-week-old B6.MRL-*Atp6v1b1*$^{vtx/vtx}$ congenic mice and much lower than those of 5-week-old MRL-*Atp6v1b1*$^{vtx/vtx}$ mice (Fig. 8A), indicating that B6-derived alleles at loci outside of the congenic region have a mostly dominant effect in preventing hearing loss. To reveal the phenotype of recessive MRL-derived, hearing loss-promoting alleles and reduce genetic complexity for mapping, the F1 hybrids were backcrossed to MRL-*Atp6v1b1*$^{vtx/vtx}$ mice rather than intercrossed. We use the notation (MRL-*vtx/vtx* x B6.MRL-*vtx/vtx*) x MRL-*vtx/vtx* to represent this backcross. N2 progeny from this backcross are homozygous for the *Atp6v1b1*^{vtx} mutation and for MRL-derived alleles at linked loci within the congenic region, but are either homozygous for MRL alleles (M/M) or heterozygous for B6 and MRL alleles (B/M) at all other loci throughout the genome. ABR thresholds of the N2 backcross mice showed a broad, non-bimodal frequency distribution (Fig. 8B) suggesting that modifier effects on hearing loss are derived from multiple loci rather than a single locus with a large effect.

We next performed a genome-wide linkage analysis of the N2 mice of the (MRL-*vtx/vtx* x B6.MRL-*vtx/vtx*) x MRL-*vtx/vtx* backcross. Out of a total of 102 N2 mice produced from this backcross (all having the *Atp6v1b1*$^{vtx/vtx}$ genotype), 20 with the lowest and 20 with the highest thresholds were chosen for the initial linkage analysis. ABR thresholds were analysed for their linkage with 120 segregating SNP markers strategically located on all chromosomes. ABR thresholds for 8-, 16-, and 32-kHz pure-tone auditory stimuli were evaluated as quantitative traits, and the MapManager QTXb20 program of least-squares linear regression (11) was used to analyse linkage associations of marker genotypes with ABR thresholds. Statistically significant linkage with ABR thresholds was found only for markers on Chr 13, with a maximum LOD score of 5.2 (Fig. 9A).

To verify and refine this linkage, we analysed all 102 N2 mice for six SNP markers spanning Chr 13 using an interval mapping approach (Fig. 9B). The most likely candidate region for modifier gene(s) on this chromosome was found to be between *rs3719347* (39.5 Mb position, GRCm38) and *rs3023390* (96.7 Mb), with *rs3654821* (63.1 Mb) having the highest association (LOD 5.4 for 16 kHz thresholds). Segregation at this locus accounts for about 20% of the total threshold variation in the backcross mice. Interval mapping in 1 cM increments showed that slightly higher associations (max LOD 6.1) could be obtained for hypothetical loci about 8 cM on either side of *rs3654821* (Fig. 9B). ABR thresholds of backcross mice homozygous for MRL-derived alleles (genotype M/M) at the *rs3654821* locus were about 20 dB higher than those of mice heterozygous for B6 and MRL alleles (genotype B/M, Fig. 9C). Mean thresholds of mice with B/M ($N = 50$) and M/M ($N = 52$) *rs3654821* genotypes were statistically significantly different at all test frequencies (two-tailed Student's t-Test probabilities < 0.00001).

The most likely location for the Chr 13 modifier of hearing loss in the backcross mice is in the 39.5–96.7 Mb region (Fig. 9B). Within this large 57 Mb region, which contains about 400 protein-coding genes, we selected two candidates for further testing, *Slc9a3* and *Slc12a7*, because they are expressed in the inner ear and are known to be involved in ion homeostasis. Strong expression of the sodium hydrogen exchanger NHE3 (the protein encoded by *Slc9a3*) was demonstrated in the apical membrane of strial marginal cells (12), and H^+ flux from this exchanger may play a role in controlling acid–base balance in cochlear endolymph (13). A knockout mutation of *Slc12a7*, which encodes the KCC4 member of the K^+-Cl^- cotransporter family, was shown to cause deafness and renal tubular acidosis; however, the endolymphatic compartments of *Slc12a7*$^{-/-}$ inner ears were not enlarged (14). We sequenced the 16 exons of *Slc9a3* and the 24 exons of *Slc12a7* along with their flanking splice sites in DNA from MRL mice and compared them to the reference sequence of the B6 strain, but found no differences except for two synonymous SNP variants detected in exons 11 and 13 of *Slc9a3*, which previously have been identified in other inbred strains.

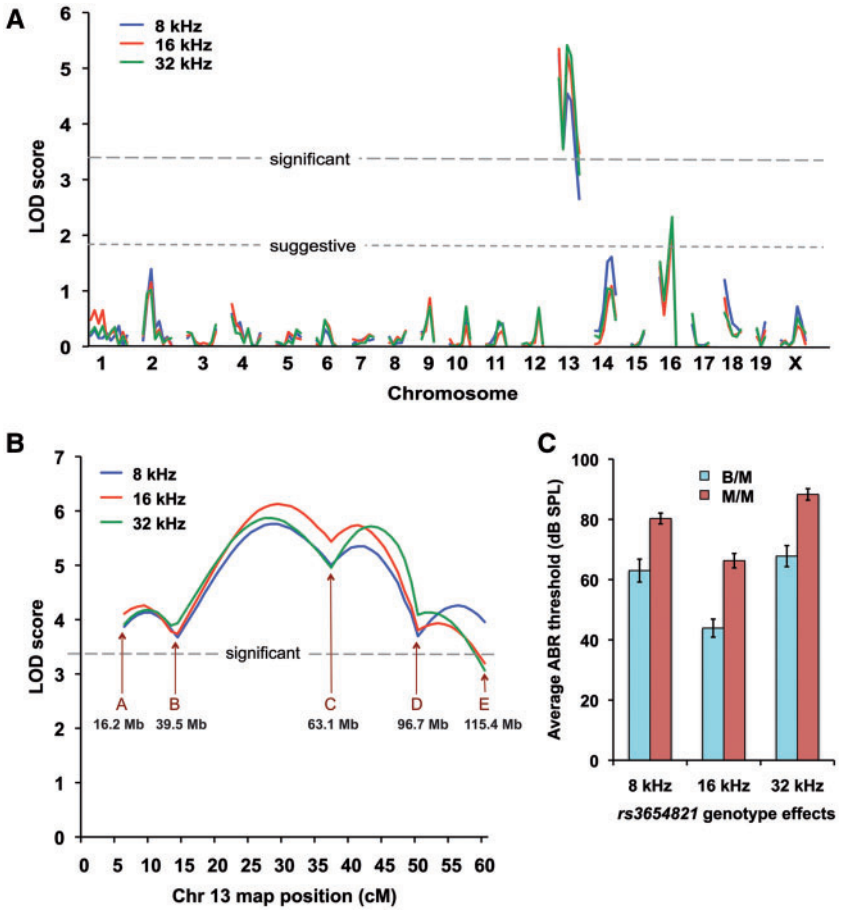

Figure 9. Mapping modifier loci that influence ABR thresholds of *Atp6v1b1*$^{vtx/vtx}$ mice. (**A**) Genome-wide linkage associations of chromosomal markers with ABR thresholds. A subset of 40 N2 mice with extreme thresholds - 20 N2 mice with the lowest and 20 with the highest - were selected for the initial genome linkage screen. Different colors are used to indicate 8 kHz, 16 kHz, and 32 kHz threshold associations with marker loci. Horizontal dashed lines mark the minimum LOD score values for suggestive and significant linkage. Only markers on Chr 13 showed a significant association with ABR thresholds. (**B**) Linkage associations of Chr 13 markers with ABR thresholds of all 102 N2 mice. The effects of a hypothetical QTL were analysed at the position of each marker locus and at 1 cM intervals between the marker loci. SNP marker loci and their Mb positions on Chr 13 are as follows: A *rs3701757*, 16.2 Mb; B *rs3719347*, 39.5 Mb; C *rs3654821*, 63.1 Mb; D *rs3023390*, 96.7 Mb; E *rs3724755*, 115.4 Mb. (**C**) Genotype effects of the Chr 13 SNP marker *rs3654821* on the mean ABR thresholds (±SEM) of the 102 backcross mice. The *rs3654821* SNP was the marker with the highest linkage association, and variation at this locus can explain about 20% of the total ABR threshold variation observed among the 102 N2 mice. B/M, heterozygous for B6 and MRL alleles ($N = 50$): M/M, homozygous for MRL alleles ($N = 52$). The mean ABR thresholds of B/M and M/M mice were statistically significantly different ($P < 0.0001$, Student's paired t-test with two-tailed distribution) for all test frequencies.

The two candidate genes also were examined by quantitative RT-PCR to evaluate and compare their mRNA expression levels in inner ear tissue of MRL and B6 mice at 2 weeks of age. We did not detect any differences in expression levels of these genes between MRL and B6 mice using the comparative delta-Ct method. The calculated fold changes (relative to the mean B6 value) in *Slc12a7* expression were 0.94 (range 0.78–1.13) for MRL and 1.00 (range 0.59–1.68) for B6, and the mean delta Ct values were not significantly different ($P = 0.81$). The calculated fold changes in *Slc9a3* expression were 1.04 (range 0.77–1.41) for MRL and 1.00, (range 0.82–1.22) for B6, and the mean delta Ct values were not significantly different ($P = 0.87$).

Discussion

We present six lines of evidence in support of the *Atp6v1b1* p.G78D missense mutation as the pathogenic variant underlying the *vtx/vtx* phenotype. 1) The *vtx* mutation was mapped to a 31 Mb chromosomal region that includes the *Atp6v1b1* gene. 2) There was complete concordance of the *vtx/vtx* phenotype with homozygosity for the *Atp6v1b1* missense mutation in all mice examined. 3) Because *vtx* is a new spontaneous mutation that occurred on the genetically homogenous MRL inbred strain, the *Atp6v1b1* missense mutation is expected to be the only DNA difference with the parental MRL strain, thereby precluding the possibility of linkage disequilibrium with other variants. 4) The inner ear phenotype of *vtx/vtx* mice is very similar to that of mice with a knockout mutation of *Atp6v0a4*$^{-/-}$, a gene that also encodes a vH^+-ATPase subunit expressed in the inner ear. 5) The glycine altered by the *Atp6v1b1*^{vtx} missense mutation is evolutionarily highly conserved, and both the SIFT (http://sift.jcvi.org/) and PolyPhen 2 (http://genetics.bwh.harvard.edu/pph2/) computer programs predict that the p.G78D substitution is probably damaging to protein function. 6) Members of two different Turkish families who present with dRTA and sensorineural hearing loss are homozygous for a missense mutation of the corresponding amino acid (p.G78R) in the human ATP6V1B1 protein (15,16).

Evidence from rat kidney cell culture experiments suggests that point mutations in B1 subunits may cause dysfunction by

inhibiting the normal trafficking of vH$^+$-ATPase to the apical membrane (17). If mutant B1 subunits cannot assemble into the native vH$^+$-ATPase complex, they might compete for molecules necessary for trafficking of the compensatory B2 subunit to the apical membrane (10). If so, the *vtx* missense mutation might be more damaging than the knockout mutation, and this may account for the phenotypic differences between *Atp6v1b1*$^{-/-}$ and *Atp6v1b1*$^{vtx/vtx}$ mutant mice. Alternatively, strain background differences may be responsible for their different phenotypes. The *Atp6v1b1*$^{-/-}$ knockout mouse with normal hearing was characterized on a mixed B6/129S1 strain background (8), whereas the *Atp6v1b1*$^{vtx/vtx}$ mutant mouse was initially characterized on an MRL strain background. To directly test the effect of strain background on the phenotype of *Atp6v1b1*$^{vtx/vtx}$ mutant mice, we developed a congenic strain in which the MRL-*Atp6v1b1*^{vtx} mutation was transferred to the B6 background. After ten generations of backcrossing (N10), the B6.MRL-*Atp6v1b1*^{vtx} congenic strain is theoretically 99.9% identical to the B6 host strain except for the linked region surrounding *Atp6v1b1*. ABR threshold measurements of the resulting B6.MRL-*Atp6v1b1*$^{vtx/vtx}$ congenic strain mice demonstrated that they have normal hearing like B6(129S1)-*Atp6v1b1*$^{-/-}$ knockout mice. We conclude from these results that strain background differences are responsible for the different auditory phenotypes of MRL-*Atp6v1b1*$^{vtx/vtx}$ mice and B6(129S1)-*Atp6v1b1*$^{-/-}$ knockout mice.

The inner ear phenotype of MRL-*Atp6v1b1*$^{vtx/vtx}$ mice (Figs 3–5) is very similar to the inner ear phenotypes of *Atp6v0a4*$^{-/-}$ (6), *Foxi1*$^{-/-}$ (18), and *Slc26a4*$^{-/-}$ (19) mice; all exhibit increased endolymph volume, loss of endocochlear potential, hearing impairment, deficient and abnormal otoconia, and vestibular dysfunction. *Foxi1* is a forkhead transcription factor that regulates expression of *Slc26a4* (18) and the *Atp6v1b1* and *Atp6v0a4* genes encoding vH$^+$-ATPase subunits in the endolymphatic sac (ES) epithelia (20). Mutations of these genes impede fluid absorption in the ES causing endolymph build up and dilatation of the membranous labyrinth (21,22); however, the molecular mechanisms underlying these effects are not fully understood. According to one proposed mechanism (21), mutations of these genes reduce the ES epithelium-generated H$^+$ current that normally forces Na$^+$ transport and fluid movement out of the ES lumen. The hearing loss, vestibular dysfunction, and other inner ear abnormalities of these mutant mice are thought to be consequences of this disrupted fluid homeostasis in the ES during embryonic development (22).

Paintfills of the membranous labyrinths of P1 inner ears of MRL-*Atp6v1b1*$^{vtx/vtx}$ mice (Fig. 3B) and P0 inner ears of *Atp6v0a4*$^{-/-}$ mice (6) show a similar morphology with greatly expanded endolymphatic sac and cochlear duct. While cochlear cross sections of P0 *Atp6v0a4*$^{-/-}$ mice show expansion of scala media, reduced scala vestibuli, and distended Reissner's membrane consistent with increased endolymph volume, cochlear cross sections of adult (2.5–4.5 month-old) MRL-*Atp6v1b1*$^{vtx/vtx}$ mice (Fig. 4) do not show these features, although they do show an overall increase in the dimensions of the cochlear capsule. One hypothesis to explain these differences is that an enlarged capsule was formed during the period when the membranous labyrinth was in an expanded state (Fig. 3B), followed by a subsequent reduction in endolymph volume at older ages (perhaps after loss of stria vascularis function), resulting in reduced size of the scala media and non-distended Reissner's membrane (Fig. 4). Based on appearance (Fig. 5), it is possible that MRL-*Atp6v1b1*$^{vtx/vtx}$ mutant cristae function normally if K$^+$ levels are normal, since the endolymphatic potential is normally low in the vestibular organs. The maculae, however, are likely unresponsive due to the lack of normal otoconia, despite little apparent hair cell loss.

Although MRL-*Atp6v1b1*$^{vtx/vtx}$ mice have malformed and dysfunctional inner ears, kidney dysfunction is minimal (Fig. 7, Table 1). The mild renal phenotype (compensated acidosis) of MRL-*Atp6v1b1*$^{vtx/vtx}$ and B6.MRL-*Atp6v1b1*$^{vtx/vtx}$ mice is similar to that reported for B6-*Atp6v1b1*$^{-/-}$ mice (8). A compensatory membrane expression of the B2 subunit of the vH$^+$-ATPase complex was proposed to explain why B6-*Atp6v1b1*$^{-/-}$ mice are healthy and do not exhibit the overt metabolic acidosis characteristic of dRTA patients with *ATP6V1B1* mutations (8), and this explanation may also apply to MRL-*Atp6v1b1*$^{vtx/vtx}$ and B6.MRL-*Atp6v1b1*$^{vtx/vtx}$ mice. In contrast, the severe metabolic acidosis reported for *Atp6v0a4*$^{-/-}$ mice (6) may be a consequence of the inability of other vH$^+$-ATPase subunits to compensate for the a4 subunit deficiency.

Although similar, the urine pH measurements for both the *Atp6v1b1*$^{vtx/vtx}$ and wildtype mice were lower compared to the previously described values by Finberg *et al.* (8). It is important to point out that the standard of care at The Jackson Laboratory is to provide mice with acidified (pH 2.5–3.0) water, and mice are therefore under an acid load, which might explain the urine pH difference. As previously reported for *Atp6v1b1* (8) and *Atp6v0a4* (7) knockout mice, *Atp6v1b1*$^{vtx/vtx}$ mice on both the B6 and MRL genetic backgrounds are hypocalciuric, which is opposite to the hypercalciuria reported for human patients with mutations in these genes (23).

There was no significant difference in urine pH between *Atp6v1b1*$^{vtx/vtx}$ and wildtype mice on the MRL background, but compared to all other strains we measured, MRL wildtype mice have more alkaline urine, with a pH that is comparable to that of *Atp6v1b1*$^{vtx/vtx}$ mutant mice on either the B6 or MRL background. A possible explanation is that the MRL strain has a mutation in a gene involved in the regulation of urine pH and that this is epistatic to the *Atp6v1b1*^{vtx} mutation. If this is indeed the case, then the much larger effect of the *Atp6v1b1*^{vtx} mutation on calcium excretion in the MRL background (70% decrease) compared to the B6 background (20% decrease) suggests a synergistic interaction of the mutations on this phenotype.

Levels of K$^+$ and Cl$^-$ in the blood did not differ between *Atp6v1b1*$^{vtx/vtx}$ and wildtype mice on either the MRL or B6 strain background (Table 1), which agrees with the findings for the *Atp6v1b1*$^{-/-}$ knockout mouse with compensated acidosis (8). In contrast, the *Atp6v0a4*$^{-/-}$ mouse with severe metabolic acidosis has significantly lower concentrations of K$^+$ and Cl$^-$ in the blood than controls (7). Although the mild renal phenotype of MRL-*Atp6v1b1*$^{vtx/vtx}$ mice is similar to that of *Atp6v1b1*$^{-/-}$ mice, its severe inner ear phenotype is similar to that of *Atp6v0a4*$^{-/-}$ mice. The difference in severity between the inner ear and kidney phenotypes of MRL-*Atp6v1b1*$^{vtx/vtx}$ mice may be due to modifying genetic factors that have stronger effects on H$^+$ transport and ion homeostasis in the inner ear than in the kidney tubule. Not all cases of dRTA caused by *ATP6V1B1* mutations have associated hearing loss (4), which lends support to the idea that inner ear and kidney-related pathologies are not always coupled.

In an attempt to identify genetic factors that contribute to the different inner ear phenotypes of MRL-*Atp6v1b1*$^{vtx/vtx}$ and B6.MRL-*Atp6v1b1*$^{vtx/vtx}$ mice, we analysed ABR threshold associations in a linkage backcross involving these two strains. Thresholds of *Atp6v1b1*$^{vtx/vtx}$ progeny from the backcross showed a broad distribution with mostly intermediate values rather than a bimodal distribution with two discreet groupings of more extreme values (Fig. 8B), indicating contributions from

multiple genes. The large variation and wide range of ABR thresholds observed in genetically identical MRL-*Atp6v1b1*$^{vtx/vtx}$ x B6.MRL-*Atp6v1b1*$^{vtx/vtx}$ F1 hybrids (Fig. 8) demonstrates discordance between genotype and phenotype that also contributed to the difficulty in mapping modifier genes. A genome-wide linkage screen detected statistically significant associations only with Chr 13 markers (Fig. 9A), but even the highest association at this locus could account for only about 20% of the total ABR threshold variation in the backcross mice. Together, these results suggest a complex genetic basis for the difference in MRL and B6 strain background effects on hearing thresholds of *Atp6v1b1*$^{vtx/vtx}$ mice, with multiple contributing genes each having relatively small effects.

We examined two interesting candidate modifier genes with known roles in inner ear fluid homeostasis (*Slc9a3* and *Slc12a7*) that lie within the candidate region of Chr 13 (39.5–96.7 Mb; Fig. 9B), but did not find any differences in the DNA sequences of their exons or in their mRNA expression levels in P14 inner ear tissue. Although our inner ear dissections did not include the endolymphatic sac, neither candidate gene shows expression in this tissue; *Slc9a3* being limited to the stria vascularis (12) and *Slc12a7* to the stria vascularis and organ of Corti supporting cells (14). Our results, however, do not rule out the possibility that non-coding sequence differences in these genes might cause subtle expression differences during inner ear development that we did not detect in two-week-old mice. Of course, one or more of the many other genes in the candidate region could also be responsible for the Chr 13 modifier effect. For example, the uncharacterized *Atp6ap1l* gene is predicted to encode a protein with similarities to ATP6AP1, an accessory subunit of the vH^+-ATPase complex, which has been implicated as a regulator of vH^+-ATPase function in the neuroendocrine secretory pathway (24), suggesting the possibility that ATP6AP1L may play a similar regulatory role in the inner ear.

Urine pH and calcium excretion were not measured in the linkage backcross mice although they showed significant differences between strains and genotypes (Fig. 7), and it is possible these differences may co-vary with ABR thresholds. If so, then genes located in the Chr 13 candidate region that are not known to affect inner ear function but are known to play a role in kidney function, such as *Slc34a1*, may also be considered as candidate modifiers of the *Atp6v1b1* phenotype.

Our results clearly establish that genetic background differences can have a profound effect on the auditory phenotypes associated with *Atp6v1b1* mutations in mice and suggest that similar genetic background effects could contribute to the phenotypic variability associated with human *ATP6V1B1* mutations. Human cases of dRTA are reported to have variable degrees of inner ear abnormalities (25) and hearing loss (4). Determining the genetic causes underlying the phenotypic differences among mouse *Atp6v1b1* mutations on different strain backgrounds may shed light on the underlying causes of this clinical heterogeneity.

Enlargement of the vestibular aqueduct (EVA, OMIM 600791), the bony canal that encloses the endolymphatic duct, is a common inner ear malformation diagnosed in children with hearing loss (https://www.nidcd.nih.gov/health/enlarged-vestibular-aqueducts-and-childhood-hearing-loss). High resolution computed tomography studies have detected bilaterally enlarged vestibular aqueducts in patients with autosomal recessive dRTA and deafness (25,26). The combination of EVA and hearing loss is also characteristic of several other syndromes, including Pendred, branchio-oto-renal, CHARGE, and Waardenburg syndromes (27). Pendred syndrome, caused by mutations of *SLC26A4*, does not always present with thyroid goiter, and these cases constitute the major known underlying cause of nonsyndromic EVA and hearing loss. Because 50% of European or North American Caucasian individuals with EVA-associated hearing loss have no obvious *SLC26A4* mutations (28), mutations of other as yet unidentified genes are thought to be responsible for some of the remaining unknown cases. Variants of *KCNJ10* and *FOXI1* have been proposed to underlie some of these cases (29,30), but contradictory results have been reported in other studies (31–33). MRL-*Atp6v1b1*$^{vtx/vtx}$ mutant mice are deaf with enlarged endolymphatic compartments of the inner ear but do not recapitulate the overt metabolic acidosis characteristic of dRTA. They thus provide a new genetic model for nonsyndromic deafness with EVA and suggest that mutations in the human *ATP6V1B1* gene might account for some of the unknown genetic cases of this disorder that are not associated with *SLC26A4* mutations.

Materials and Methods

Mice

Experimental mice were bred and housed in the Research Animal Facility of the Jackson Laboratory in Bar Harbor, Maine. Mice were fed *ad libitum* with a 6% fat mouse diet. Water bottles were changed weekly and filled with acidified (pH 2.5–3.0) water. The light cycle was 12-h light and 12-h dark. Some post-weaning mice were shipped to Washington University in St. Louis, Missouri, for additional analyses. All procedures involving the use of experimental mice were approved by the Institutional Animal Care and Use Committees at The Jackson Laboratory and Washington University. All methods used in the study were performed in accordance with the guidelines and regulations of the U.S. National Institutes of Health (NIH) Office of Laboratory Animal Welfare (OLAW) and the Public Health Service (PHS) Policy on the Humane Care and Use of Laboratory Animals.

The vortex (*vtx*) mutation arose spontaneously on strain MRL/MpJ-*Fas*^{lpr}/J (JAX Stock #485). The *Fas*^{lpr} mutation was subsequently removed from the *vtx* colony by mating *vtx/vtx* mice with MRL/MpJ (Stock #486) mice and selecting progeny without the *Fas*^{lpr} mutation as founders. The resulting strain is designated MRL/MpJ-*Atp6v1b1*^{vtx}/KjnJ (Stock #21771), here abbreviated MRL-*Atp6v1b1*^{vtx}. Mutant mice (*vtx/vtx*) can be identified without genotyping by their overt circling and head tilting behaviors, and the colony is maintained by mating +/*vtx* (unaffected) x *vtx/vtx* (affected) mice. Both female and male *vtx/vtx* mice of the MRL-*Atp6v1b1*^{vtx} strain are fertile and able to breed.

A C57BL/6J (B6) congenic strain carrying the *vtx* mutation was generated by first mating MRL-*Atp6v1b1*$^{vtx/vtx}$ mice with B6 mice to produce F1 hybrids, followed by repeated backcrosses to B6 mice, at each generation selecting hybrids heterozygous for the MRL-derived *Atp6v1b1*^{vtx} mutation (inferred by the presence of MRL alleles at flanking markers *D6Mit144* and *D6Mit29*). N10 generation *Atp6v1b1*$^{+/vtx}$ mice were then inbred, and the MRL-derived *Atp6v1b1*$^{vtx/vtx}$ genotype was verified by DNA sequencing. The resulting homozygous congenic strain is designated B6.MRL-*Atp6v1b1*^{vtx}/KjnJ (Stock #21772), here abbreviated B6.MRL-*Atp6v1b1*^{vtx}. To define the extent of the congenic region, 19 SNP markers along the length of Chromosome 6 were genotyped for B6 and MRL alleles, and the 74-84 Mb MRL-derived congenic region of B6.MRL-*Atp6v1b1*^{vtx} was determined to extend from a breakpoint between *rs13478686* (Chr6: 29,712,455; GRCm38) and *rs3023067* (Chr6: 36,019,022) to a breakpoint between *rs3024107* (Chr 6: 109,859,726) and *rs3693392* (Chr 6: 113,320,611).

Genetic mapping and DNA analysis of the *vtx* mutation

To genetically map the *vtx* mutation, individual DNA samples from linkage cross mice were typed for multiple MIT microsatellite markers located throughout the mouse genome. Previously described PCR methods (34) were used to genotype the chromosomal markers, which were then analysed for co-segregation with the mutant phenotype. PCR primer pairs designed to amplify specific markers were purchased from Integrated DNA Technologies (Coralville, IA, USA).

PCR for comparative DNA analysis between *vtx/vtx* mutant and control mice was performed according to the same conditions as described above for genetic mapping. PCR primers used to identify the *vtx* mutation of the *Atp6v1b1* gene for genotyping were 5'- GATCCCCTTCTCCACATCAG -3' (forward) and 5'- AGCATGGTCTATGTGCTGGG -3' (reverse). The expected PCR product size (590 bp) was confirmed on a 3.5% agarose gel. PCR products then were purified with the QIAquick PCR Purification Kit (Qiagen Inc., Valencia, CA), and sequenced on an Applied Biosystems 3700 DNA Sequencer with an optimized Big Dye Terminator Cycle Sequencing method. Typical DNA sequencing results for distinguishing *Atp6v1b1* wildtype and *vtx* mutant alleles are shown in Figure 2A.

Auditory brainstem response (ABR) measurements

At the Jackson Laboratory, ABR thresholds were measured at 8, 16 and 32 kHz in a sound attenuating chamber using the SmartEP auditory evoked potential diagnostic system from Intelligent Hearing Systems (IHS, Miami, FL) as described previously (35). Briefly, mice were anesthetized with tribromoethanol (0.2 ml of 20 mg/ml stock per 10 g of body weight, i.p.) and placed on a temperature controlled heating pad to maintain body temperature at 37° C. Output tubes from high frequency transducers were snugly fit in the ear canals of the mouse. Both ears were tested simultaneously, which effectively measures the thresholds of the better responding ear. Three subdermal electrodes, placed at the vertex and behind each ear, were used to record brain stem responses to defined tone-bursts (3 ms duration. 1.5 ms cosine-gated rise/fall time). The responses were then amplified, filtered (100–3000 Hz) and averaged (25 kHz sampling rate, 10 ms analysis window). Stimulus intensity was initially decreased in 10 dB steps until the response began to disappear and then lowered in 5 dB steps; ABR threshold was defined as the lowest intensity at which an ABR response could be reliably obtained. With our testing system, average ABR thresholds for normal hearing mice are about 40, 20, and 45 dB SPL for 8, 16 and 32 kHz stimuli, respectively. Data from ABR tests at the Jackson Laboratory are shown in Figures 1 and 8.

At Washington University School of Medicine (WUSM), ABR measurements were performed in a foam-lined, single-walled soundproof room (IAC). Animals were anesthetized (80 mg/kg ketamine, 15 mg/kg xylazine, IP) and positioned dorsally in a custom head holder. Core temperature was maintained at 37.5 ± 1.0 °C using a DC electric heating pad in conjunction with a rectal probe (FHC). Platinum needle electrodes (Grass) were inserted subcutaneously just behind the right ear (active), at the vertex (reference), and in the back (ground). Electrodes were connected to a Grass P15 differential amplifier (300–3,000 Hz, ×100), then to a custom amplifier providing another 1,000X gain, then digitized at 30 kHz and visualized using Tucker Davis Technologies (TDT) System 2 hardware and software. Sine wave stimuli having 0.5 ms $\cos^2$ rise/fall times and 5.0 ms total duration were also generated and calibrated using TDT System2 hardware and software. Stimuli were presented free-field using TDT ES-1 speakers placed 7.0 cm from the left pinna and calibrated offline using an ACO Pacific 7016 ¼ inch microphone placed where the external auditory meatus would normally be. During ABR tests, tone burst stimuli at each frequency and level were presented up to 1,000 times at 20/s. The minimum sound pressure level (SPL) required for visual detection of ABR Wave I was determined at 5, 10, 20, 28.3, 40 and 56.6 kHz using a 5 dB minimum step size. Data from ABR tests at WUSM are shown in Figure 6.

Endocochlear potential (EP) recording

EP recordings were performed at WUSM. Using a fine drill, a hole was made in the left cochlear capsule directly over scala media of the lower basal turn. Glass capillary pipettes (40–80 MΩ) filled with 0.15 M KCl were mounted on a hydraulic microdrive (Frederick Haer) and advanced until a stable positive potential was observed that did not change with increased electrode depth. The signal from the recording electrode was led to an AM Systems Model 1600 intracellular amplifier. A total 23 EP measurements were made, including 8 from MRL-*Atp6v1b1*$^{vtx/vtx}$ mice. In later light microscopic examinations of left cochleae it was determined that 4 of the 8 measurements from MRL-*Atp6v1b1*$^{vtx/vtx}$ mice had missed the scala media, owing to displacement of stria vascularis behind the stapedial artery. This shift was observed only in MRL-*Atp6v1b1*$^{vtx/vtx}$ mice, apparently as part of a reshaping of the fluid spaces by the mutation.

Tissue processing and imaging for histopathology

At the end of ABR and EP recordings at WUSM, animals were overdosed and perfused transcardially with cold 2.0% paraformaldehyde/2.0% glutaraldehyde in 0.1 M phosphate buffer (pH 7.4). Each cochlea was rapidly isolated, immersed in the same fixative, and the stapes was immediately removed. After decalcification in sodium EDTA for 72 h, cochleae were post-fixed in buffered 1% osmium tetroxide, dehydrated in an ascending acetone series, and embedded in Epon. Cochleae were sectioned parallel to the modiolus at 4.0 μm, then stained with toluidine blue for bright field viewing. All auditory and vestibular epithelia were examined qualitatively in initially three inner ears (three animals) per genotype. Due to the heterogeneity in appearance of the inner ears of MRL-*Atp6v1b1*$^{vtx/vtx}$ mice, 9 were examined in serial detail, so that central tendencies could be discerned. Bright field images used for illustration were obtained on a Zeiss LSM 700 laser scanning confocal microscope using ZEN™ software.

Inner ear paint fills and cleared whole mount preparations

E15 embryos (MRL-*Atp6v1b1*$^{vtx/+}$, $n = 5$; MRL-*Atp6v1b1*$^{vtx/vtx}$, $n = 6$) and P1 mice (MRL-*Atp6v1b1*$^{vtx/+}$, $n = 7$; MRL-*Atp6v1b1*$^{vtx/vtx}$, $n = 5$) were used for inner ear paint fills. E15 embryos were decapitated and whole heads were fixed in Bodian's fixative. P1 mice were decapitated and half-heads were fixed in Bodian's fixative after the brain was removed. Heads were fixed overnight and then dehydrated with 75% ethanol (2 × 2 h), 95% ethanol (2 × 2 h), and 100% ethanol (2 ×2 h). Heads were then rinsed once with methyl salicylate and cleared overnight by placing specimens in methyl salicylate. Inner ears were filled with 1%

Wite-Out correction fluid in methyl salicylate using a Hamilton syringe, with a pulled glass capillary needle broken to a tip diameter of 20–40 μm. E15 inner ears were injected through the middle turn of the cochlea. Two injections were done for P1 inner ears with one injection to the cochlear middle turn and the second injection in the common crus (Kiernan, 2006). To observe otoconia, inner ears dissected from bisected heads of P1 mice were cleared with methyl salicylate as described above, sub-illuminated and photographed using a Leica dissecting microscope.

Blood and urine analysis

At 17 weeks of age spot urine and blood were collected from 5 males of each group. Immediately after collection, urine pH was measured by using a glass pH electrode (Thermo Orion Micro pH Probe). Sodium, potassium, and chloride were measured in urine and blood, calcium and creatinine were measured in urine on a Beckman AU680 Chemistry analyzer. Osmolality of blood and urine was measured using a 5004 micro-Osmette (Precision Systems).

Genetic mapping of modifier loci

For linkage backcross analysis to map modifier loci, tail-tip samples from individual N2 progeny mice were provided to the Jackson Laboratory's Genotyping Service, which outsources SNP genotyping to LGC Genomics (Beverly MA). Each mouse DNA sample was genotyped for 120 selected SNPs that differ between the B6 and MRL strains. The ABR thresholds of the same backcross mice were evaluated as quantitative traits, and the MapManager QTXb20 program of least-squares linear regression (11) was used to analyse linkage and identify marker associations with ABR thresholds.

Analyses of candidate modifier genes

DNA and cDNA sequencing of candidate genes was performed on an Applied Biosystems 3700 DNA Sequencer with an optimized Big Dye Terminator Cycle Sequencing method, and the sequencing results were analysed with Sequencher DNA Sequence Analysis Software (Gene Codes Corporation, Ann Arbor, MI, USA).

For qRT-PCR analysis of candidate gene expression, inner ears were dissected from two-week-old MRL-*Atp6v1b1*$^{vtx/vtx}$, MRL-*Atp6v1b1*$^{vtx/+}$, B6.MRL-*Atp6v1b1*$^{vtx/vtx}$, and B6 wild-type mice and snap frozen in liquid nitrogen. Inner ear tissues did not include the endolymphatic sac, which was lost during the dissection process. The two inner ears of each mouse were pooled together and homogenized in 1 ml TRIzol (Life Technologies) in GentleMACS M-tubes (Miltenyi Biotech) using a GentleMACS dissociator. Homogenates were briefly centrifuged to pellet and remove cell debris. Homogenates were phase separated in 1/5 volume of chloroform. RNAs were extracted using the MagMAX mirVana Total RNA Isolation Kit (Life Technologies) following the manufacturer's recommendations on the KingFisher Flex Purification System (Thermo Fisher Scientific). RNA quantity and quality were assessed using a Nanodrop 2000 (Thermo Scientific) and Bioanalyzer 2100 (Agilent) respectively. RNA was reverse-transcribed into cDNA using 500 ng total RNA and the Superscript IV First-Strand Synthesis System (Thermo Fisher Scientific) following the manufacturer's recommendations. cDNA was diluted 1:5 with RNase-free water, and 2 μl of was used for quantitative real-time PCR (qPCR) using a standard SYBR green comparative Ct template on a Life Technologies ViiA7 qPCR machine. Primer sequences were ATCCTTTTCCTGCGTCTGAC-forward and CTCAT GGAGATGGCTGTCAG-reverse (110 bp product) for *Slc12a7* and AGGTGGTCACCTTCAAATGG-forward and ACCTTGTGGGACA GGTGAAA-reverse (106 bp product) for *Slc9a3*; both primer pairs produced robust single band products on agarose gels. The double delta-Ct method was used to calculate fold changes in expression levels, and statistical analysis comparing mean delta Ct values was done with the two-tailed student test.

Acknowledgements

We wish to thank Belinda Harris for her discovery of the *vtx* mutation and Sandra Gray for mouse colony management and generation of congenic and linkage cross mice.

Conflict of Interest statement. None declared.

Funding

This work was supported by the National Institutes of Health (NIH) grants R01-DC004301 (to K.R.J.), U54-OD020351, and P30-CA034196.

References

1. Lang, F., Vallon, V., Knipper, M. and Wangemann, P. (2007) Functional significance of channels and transporters expressed in the inner ear and kidney. *Am. J. Physiol. Cell Physiol.*, **293**, C1187–1C1208.
2. Karet, F.E., Finberg, K.E., Nelson, R.D., Nayir, A., Mocan, H., Sanjad, S.A., Rodriguez-Soriano, J., Santos, F., Cremers, C.W., Di Pietro, A. *et al.* (1999) Mutations in the gene encoding B1 subunit of H+-ATPase cause renal tubular acidosis with sensorineural deafness. *Nat. Genet.*, **21**, 84–90.
3. Stover, E.H., Borthwick, K.J., Bavalia, C., Eady, N., Fritz, D.M., Rungroj, N., Giersch, A.B., Morton, C.C., Axon, P.R., Akil, I. *et al.* (2002) Novel ATP6V1B1 and ATP6V0A4 mutations in autosomal recessive distal renal tubular acidosis with new evidence for hearing loss. *J. Med. Genet.*, **39**, 796–803.
4. Vargas-Poussou, R., Houillier, P., Le Pottier, N., Strompf, L., Loirat, C., Baudouin, V., Macher, M.A., Dechaux, M., Ulinski, T., Nobili, F. *et al.* (2006) Genetic investigation of autosomal recessive distal renal tubular acidosis: evidence for early sensorineural hearing loss associated with mutations in the ATP6V0A4 gene. *J. Am. Soc. Nephrol.*, **17**, 1437–1443.
5. Batlle, D. and Haque, S.K. (2012) Genetic causes and mechanisms of distal renal tubular acidosis. *Nephrol. Dial. Transplant.*, **27**, 3691–3704.
6. Lorente-Canovas, B., Ingham, N., Norgett, E.E., Golder, Z.J., Karet Frankl, F.E. and Steel, K.P. (2012) Mice deficient in the H+-ATPase a4 subunit have severe hearing impairment associated with enlarged endolymphatic compartments within the inner ear. *Dis. Model Mech.*, **6**, 434–442.
7. Norgett, E.E., Golder, Z.J., Lorente-Canovas, B., Ingham, N., Steel, K.P. and Frankl, F.E. (2012) Atp6v0a4 knockout mouse is a model of distal renal tubular acidosis with hearing loss, with additional extrarenal phenotype. *Proc. Natl Acad. Sci. U S A*, **109**, 13775–13780.
8. Finberg, K.E., Wagner, C.A., Bailey, M.A., Paunescu, T.G., Breton, S., Brown, D., Giebisch, G., Geibel, J.P. and Lifton, R.P. (2005) The B1-subunit of the H(+) ATPase is required for

maximal urinary acidification. *Proc. Natl Acad. Sci. U S A*, **102**, 13616–13621.
9. Dou, H., Finberg, K., Cardell, E.L., Lifton, R. and Choo, D. (2003) Mice lacking the B1 subunit of H+ -ATPase have normal hearing. *Hear. Res.*, **180**, 76–84.
10. Paunescu, T.G., Russo, L.M., Da Silva, N., Kovacikova, J., Mohebbi, N., Van Hoek, A.N., McKee, M., Wagner, C.A., Breton, S. and Brown, D. (2007) Compensatory membrane expression of the V-ATPase B2 subunit isoform in renal medullary intercalated cells of B1-deficient mice. *Am. J. Physiol. Renal. Physiol.*, **293**, F1915–F1926.
11. Manly, K.F., Cudmore, R.H., Jr. and Meer, J.M. (2001) Map Manager QTX, cross-platform software for genetic mapping. *Mamm. Genome*, **12**, 930–932.
12. Bond, B.R., Ng, L.L. and Schulte, B.A. (1998) Identification of mRNA transcripts and immunohistochemical localization of Na/H exchanger isoforms in gerbil inner ear. *Hear. Res.*, **123**, 1–9.
13. Miyazaki, H., Wangemann, P. and Marcus, D.C. (2016) The gastric H,K-ATPase in stria vascularis contributes to pH regulation of cochlear endolymph but not to K secretion. *BMC Physiol.*, **17**, 1.
14. Boettger, T., Hubner, C.A., Maier, H., Rust, M.B., Beck, F.X. and Jentsch, T.J. (2002) Deafness and renal tubular acidosis in mice lacking the K-Cl co-transporter Kcc4. *Nature*, **416**, 874–878.
15. Borthwick, K.J., Kandemir, N., Topaloglu, R., Kornak, U., Bakkaloglu, A., Yordam, N., Ozen, S., Mocan, H., Shah, G.N., Sly, W.S. *et al.* (2003) A phenocopy of CAII deficiency: a novel genetic explanation for inherited infantile osteopetrosis with distal renal tubular acidosis. *J. Med.Genet.*, **40**, 115–121.
16. Subasioglu Uzak, A., Cakar, N., Comak, E., Yalcinkaya, F. and Tekin, M. (2013) ATP6V1B1 mutations in distal renal tubular acidosis and sensorineural hearing loss: clinical and genetic spectrum of five families. *Ren. Fail.*, **35**, 1281–1284.
17. Yang, Q., Li, G., Singh, S.K., Alexander, E.A. and Schwartz, J.H. (2006) Vacuolar H+ -ATPase B1 subunit mutations that cause inherited distal renal tubular acidosis affect proton pump assembly and trafficking in inner medullary collecting duct cells. *J. Am. Soc. Nephrol.*, **17**, 1858–1866.
18. Hulander, M., Kiernan, A.E., Blomqvist, S.R., Carlsson, P., Samuelsson, E.J., Johansson, B.R., Steel, K.P. and Enerback, S. (2003) Lack of pendrin expression leads to deafness and expansion of the endolymphatic compartment in inner ears of Foxi1 null mutant mice. *Development*, **130**, 2013–2025.
19. Everett, L.A., Belyantseva, I.A., Noben-Trauth, K., Cantos, R., Chen, A., Thakkar, S.I., Hoogstraten-Miller, S.L., Kachar, B., Wu, D.K. and Green, E.D. (2001) Targeted disruption of mouse Pds provides insight about the inner-ear defects encountered in Pendred syndrome. *Hum. Mol. Genet.*, **10**, 153–161.
20. Vidarsson, H., Westergren, R., Heglind, M., Blomqvist, S.R., Breton, S. and Enerback, S. (2009) The forkhead transcription factor Foxi1 is a master regulator of vacuolar H-ATPase proton pump subunits in the inner ear, kidney and epididymis. *PLoS One*, **4**, e4471.
21. Kim, H.M. and Wangemann, P. (2010) Failure of fluid absorption in the endolymphatic sac initiates cochlear enlargement that leads to deafness in mice lacking pendrin expression. *PLoS One*, **5**, e14041.
22. Li, X., Sanneman, J.D., Harbidge, D.G., Zhou, F., Ito, T., Nelson, R., Picard, N., Chambrey, R., Eladari, D., Miesner, T. *et al.* (2013) SLC26A4 targeted to the endolymphatic sac rescues hearing and balance in Slc26a4 mutant mice. *PLoS Genet.*, **9**, e1003641.
23. Alexander, R.T., Cordat, E., Chambrey, R., Dimke, H. and Eladari, D. (2016) Acidosis and urinary calcium excretion: insights from genetic disorders. *J. Am. Soc. Nephrol.*, **27**, 3511–3520.
24. Jansen, E.J. and Martens, G.J. (2012) Novel insights into V-ATPase functioning: distinct roles for its accessory subunits ATP6AP1/Ac45 and ATP6AP2/(pro) renin receptor. *Curr. Protein Pept. Sci.*, **13**, 124–133.
25. Andreucci, E., Bianchi, B., Carboni, I., Lavoratti, G., Mortilla, M., Fonda, C., Bigozzi, M., Genuardi, M., Giglio, S. and Pela, I. (2009) Inner ear abnormalities in four patients with dRTA and SNHL: clinical and genetic heterogeneity. *Pediatr. Nephrol.*, **24**, 2147–2153.
26. Joshua, B., Kaplan, D.M., Raveh, E., Lotan, D. and Anikster, Y. (2008) Audiometric and imaging characteristics of distal renal tubular acidosis and deafness. *J. Laryngol. Otol.*, **122**, 193–198.
27. Pryor, S.P., Madeo, A.C., Reynolds, J.C., Sarlis, N.J., Arnos, K.S., Nance, W.E., Yang, Y., Zalewski, C.K., Brewer, C.C., Butman, J.A. *et al.* (2005) SLC26A4/PDS genotype-phenotype correlation in hearing loss with enlargement of the vestibular aqueduct (EVA): evidence that Pendred syndrome and non-syndromic EVA are distinct clinical and genetic entities. *J. Med. Genet.*, **42**, 159–165.
28. Rehman, A.U., Friedman, T.B. and Griffith, A.J. (2016) Unresolved questions regarding human hereditary deafness. *Oral Dis.* **23**, 551–558.
29. Yang, T., Gurrola, J.G., 2nd, Wu, H., Chiu, S.M., Wangemann, P., Snyder, P.M. and Smith, R.J. (2009) Mutations of KCNJ10 together with mutations of SLC26A4 cause digenic nonsyndromic hearing loss associated with enlarged vestibular aqueduct syndrome. *Am. J. Hum. Genet.*, **84**, 651–657.
30. Yang, T., Vidarsson, H., Rodrigo-Blomqvist, S., Rosengren, S.S., Enerback, S. and Smith, R.J. (2007) Transcriptional control of SLC26A4 is involved in Pendred syndrome and nonsyndromic enlargement of vestibular aqueduct (DFNB4). *Am. J. Hum. Genet.*, **80**, 1055–1063.
31. Landa, P., Differ, A.M., Rajput, K., Jenkins, L. and Bitner-Glindzicz, M. (2013) Lack of significant association between mutations of KCNJ10 or FOXI1 and SLC26A4 mutations in Pendred syndrome/enlarged vestibular aqueducts. *BMC Med. Genet.*, **14**, 85.
32. Zhao, J., Yuan, Y., Huang, S., Huang, B., Cheng, J., Kang, D., Wang, G., Han, D. and Dai, P. (2014) KCNJ10 may not be a contributor to nonsyndromic enlargement of vestibular aqueduct (NSEVA) in Chinese subjects. *PLoS One*, **9**, e108134.
33. Chen, K., Wang, X., Sun, L. and Jiang, H. (2012) Screening of SLC26A4, FOXI1, KCNJ10, and GJB2 in bilateral deafness patients with inner ear malformation. *Otolaryngol. Head Neck Surg.*, **146**, 972–978.
34. Johnson, K.R., Longo-Guess, C.M. and Gagnon, L.H. (2012) Mutations of the mouse ELMO domain containing 1 gene (Elmod1) link small GTPase signaling to actin cytoskeleton dynamics in hair cell stereocilia. *PLoS One*, **7**, e36074.
35. Zheng, Q.Y., Johnson, K.R. and Erway, L.C. (1999) Assessment of hearing in 80 inbred strains of mice by ABR threshold analyses. *Hear. Res.*, **130**, 94–107.